AIP | The Journal of Chemical Physics

Theory of adhesion: Role of surface roughness

B. N. J. Persson and M. Scaraggi

Citation: The Journal of Chemical Physics **141**, 124701 (2014); doi: 10.1063/1.4895789
View online: http://dx.doi.org/10.1063/1.4895789
View Table of Contents: http://scitation.aip.org/content/aip/journal/jcp/141/12?ver=pdfcov
Published by the AIP Publishing

Theory of adhesion: Role of surface roughness

B. N. J. Persson[1] and M. Scaraggi[1,2]
[1]*PGI, FZ-Jülich, 52425 Jülich, Germany*
[2]*DII, Universitá del Salento, 73100 Monteroni-Lecce, Italy*

(Received 13 May 2014; accepted 4 September 2014; published online 23 September 2014)

We discuss how surface roughness influences the adhesion between elastic solids. We introduce a Tabor number which depends on the length scale or magnification, and which gives information about the nature of the adhesion at different length scales. We consider two limiting cases relevant for (a) elastically hard solids with weak (or long ranged) adhesive interaction (DMT-limit) and (b) elastically soft solids with strong (or short ranged) adhesive interaction (JKR-limit). For the former cases we study the nature of the adhesion using different adhesive force laws ($F \sim u^{-n}$, $n = 1.5$–4, where u is the wall-wall separation). In general, adhesion may switch from DMT-like at short length scales to JKR-like at large (macroscopic) length scale. We compare the theory predictions to results of exact numerical simulations and find good agreement between theory and simulation results. © *2014 AIP Publishing LLC*. [http://dx.doi.org/10.1063/1.4895789]

I. INTRODUCTION

Surface roughness has a huge influence on the adhesion and friction between macroscopic solid objects.[1–6] Most interactions are short ranged and become unimportant when the separation between solid surfaces exceeds a few atomic distances, i.e., at separations of order nm. This is trivially true for chemical bonds (covalent or metallic bonds) but also holds for the more long-ranged van der Waals interaction. One important exception is charged bodies. For uncharged solids, if the surface roughness amplitude is much larger than the decay length of the wall-wall interaction potential and if the solids are elastically stiff enough, no macroscopic adhesion will prevail, as is the case in most practical cases. Only for very smooth surfaces, or elastically very soft solids (which can deform and make almost perfect contact at the contacting interface without storing up a large elastic energy) adhesion can be observed for macroscopic solids.[7]

In this paper we will discuss how surface roughness influences adhesion between macroscopic solids. We consider two limiting cases, which are valid for elastically hard and weakly interacting solids (Deryagin, Muller, and Toporov, DMT-limit)[8] and for elastically soft or strongly interacting solids (Johnson, Kendall, and Roberts, JKR-limit).[9] This problem has been studied before but usually using the Greenwood-Williamson (GW)[10,11] type of asperity models (see, e.g., Refs. 7 and 12), whereas our treatment is based on the Persson contact mechanics theory. The latter theory is (approximately) valid even close to complete contact (which often prevails when adhesion is important).[13,14]

For surfaces with roughness on many length scales (as is always the case in reality) the GW-type of asperity contact models, even when one includes the long-range elastic lateral coupling between the asperities, are not valid. First, one cannot approximate all the asperities as spherical (or ellipsoidal) cups with the same radius of curvature as done in the GW theory. Also, in many adhesion problems the contact is almost complete, and for this limit the GW theory fails qualitatively.

Asperity models can only be used as long as the contact area is small compared to the nominal contact area, and even in this limit these models have severe problems for surfaces with roughness on many length scales.[15–17]

Recently, several numerical simulation studies of adhesion between randomly rough surfaces have been published. Pastewka and Robbins[18] studied the adhesion between rough surfaces in the DMT-limit, and presented a criterion for macroscopic adhesion. They emphasized the role of the range of the adhesive interaction, which we also find is important in the DMT-limit and when the surface roughness amplitude is small (see below). Medina and Dini[19] studied the adhesion between an elastic sphere with smooth surface and a rigid randomly rough substrate surface. They observed strong contact hysteresis in the JKR-limit (relative smooth surfaces) and very small contact hysteresis in the DMT-limit which prevails for small roughness. Analytical theories of contact mechanics have been compared to Molecular Dynamics calculations for an elastic ball in contact with two-dimensional (2D) randomly rough surfaces in Ref. 20. Numerically exact studies for adhesion between 1D surface roughness was presented in Ref. 21. Experimental adhesion data for rough surfaces have been compared to analytical theory predictions in Refs. 22–24.

In this paper we present a more general study for the adhesive contact between solids with nominal flat but randomly rough surfaces, for a large range of system parameters. Exact simulation results are compared to theory predictions in both the JKR and DMT limits, but with the main focus on the DMT limit. We also introduce a scale-dependent Tabor number which gives information about the condition for the validity of the DMT and JKR limits. For macroscopic solids one expect in many cases that the JKR limit is accurate for the contact mechanics at long length scales, but the DMT-limit

may still prevail at short length scales (for small asperity-contact regions).

Many practical or natural adhesive systems involve effects which usually are not considered in adhesion models, and which we will not address in this paper. In particular, biological applications typically involve complex structured surfaces (e.g., hierarchical fiber-and-plate structures) with anisotropic elastic properties, which are elastically soft on all relevant length scales.[25–28] Instead of directly relying on molecular bonding over atomic dimension, many biological systems adhere mainly via capillary bridges.[29–31] We will also not discuss either the adhesion between charged objects, which must be treated by special methods which takes into account the long-range nature of the Coulomb interaction.[32–35]

In this paper we first briefly review (Sec. II) two limiting models of adhesion for smooth surfaces. In Sec. III we show how the same limiting cases can be studied analytically for randomly rough surfaces using the Persson contact mechanics model. Numerical results obtained using the analytical theory are presented in Sec. IV, and compared to simulation results in Sec. V. Section VI contains a discussion and Sec. VII contains the summary and conclusion.

II. ADHESION OF BALL ON FLAT (REVIEW)

Analytical studies of adhesion have been presented for smooth surfaces for bodies of simple geometrical shape, the most important case being the contact between spherical bodies. For a sphere in contact with a flat surface two limiting cases are of particular importance, usually referred to as the DMT theory[8] and the JKR theory,[9] see Fig. 1. Analytical results for intermediate-range adhesion were presented by Maugis[36,37] and the ball-flat adhesion problem has also been studied in detail using numerical methods.[38,39] A particularly detailed simulation study was recently published by Müser who also included negative work of adhesion (repulsive wall-wall interaction).[40]

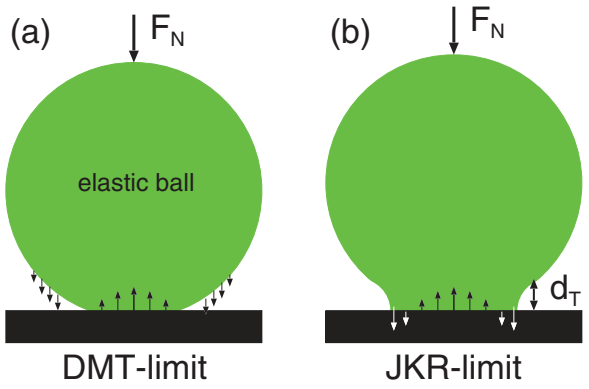

FIG. 1. (a) In the DMT theory the elastic deformation field is calculated with the adhesion included only as an additional load F_{ad} acting on the sphere. Thus the contact area is determined by Hertz theory with the external load $F_N + F_{ad}$. The adhesive load F_{ad} is obtained by integrating the adhesive stress over the ball non-contact area. (b) In the JKR theory the adhesion force is assumed to have infinitesimal spatial extent, and is included only in the contact area as an interfacial binding energy $E_{ad} = \Delta\gamma A$. The shape of the elastic body is obtained by minimizing the total energy $-E_{ad} + U_{el}$, where U_{el} is the elastic deformation energy.

Consider an elastic ball (e.g., a rubber ball) with the radius R, Young's elastic modulus E (and Poisson ratio ν), in adhesive contact with a flat rigid substrate. Let $\Delta\gamma = \gamma_1 + \gamma_2 - \gamma_{12}$ be the Dupré's work of adhesion and let d_c be the spatial extent of the wall-wall interaction potential (typically of order atomic distance). The DMT theory is valid when adhesive stress $\sigma_{ad} \approx \Delta\gamma/d_c$ is much smaller than the stress in the contact region, which is of order

$$\sigma_c \approx \left(\frac{\Delta\gamma E^2}{R}\right)^{1/3}.$$

In the opposite limit the JKR theory is valid. In the DMT theory the elastic deformation field is calculated with the adhesion included only as an additional load F_{ad} acting on the sphere. Thus the contact area is determined by Hertz theory with the external load $F_0 = F_N + F_{ad}$, where F_N is the actual load on the ball (see Fig. 1). The adhesion load F_{ad} is obtained by integrating the adhesion stress over the ball non-contact area.

The JKR theory neglects the extent of the interaction potential and assumes interaction between the solids only in the contact area. The deformation field in the JKR theory is obtained by minimizing the total energy given by the sum of the (repulsive) elastic deformation energy and the (attractive) binding energy $E_{ad} = \Delta\gamma A$, where A is the contact area. In this theory the contribution to binding energy from the non-contact region is neglected.

Since $\sigma_{ad} \approx \Delta\gamma/d_c$ we can define the Tabor number:

$$\mu_T = \frac{\sigma_{ad}}{\sigma_c} = \left(\frac{R\Delta\gamma^2}{E_r^2 d_c^3}\right)^{1/3} = \frac{d_T}{d_c},$$

where

$$d_T = \left(\frac{R\Delta\gamma^2}{E_r^2}\right)^{1/3},$$

where $E_r = E/(1-\nu^2)$ is the effective elastic modulus. The DMT and JKR limits correspond to $\mu_T \ll 1$ and $\mu_T \gg 1$, or, equivalently, $d_T \ll d_c$ and $d_T \gg d_c$, respectively. In the JKR-limit the Tabor length d_T can be considered as the height of the neck which is formed at the contact line (see Fig. 1(b)). This neck height must be much larger than the length d_c, which characterizes the spatial extent of the wall-wall interaction, in order for the JKR-limit to prevail.

At vanishing external load, $F_N = 0$, the JKR theory predicts the contact area:

$$A_{JKR} = \pi\left(\frac{9\pi R^2\Delta\gamma}{2E_r}\right)^{2/3}.$$

This contact area is a factor $3^{2/3} \approx 2.1$ larger than obtained from the DMT theory. In the JKR theory the force necessary to remove the ball from the flat (the pull-off force) is given by

$$F_c = \frac{3\pi}{2}\Delta\gamma R \quad (1)$$

which is a factor of 3/4 times smaller than predicted by the DMT theory. Also the pull-off processes differ: in the JKR theory an elastic instability occurs where the contact area abruptly decreases, while in the DMT theory the contact area decreases continuously, until the ball just touches

the substrate in a single point, at which point the pull-force is maximal.

For the sphere-flat case the pull-off force in the DMT-limit is *independent* of the range of the wall-wall interaction potential. However, this is not the case for other geometries where in fact the contact mechanics depends remarkably sensitively on the interaction range. As a result the interaction between rough surfaces in the DMT-limit will depend on the force law as we will demonstrate below for power law interaction $p_{\rm ad} \sim u^{-n}$.

In an exact treatment, as a function of the external load $F_{\rm N}$, the total energy $E_{\rm tot} = -E_{\rm ad} + U_{\rm el}$ must have a minimum at $F_{\rm N} = 0$. This is the case in the JKR theory but in general not for the DMT theory. Instead, the DMT theory is only valid for very stiff solids and in this limiting case the total energy minimum condition is almost satisfied. Nevertheless, one cannot expect $dE_{\rm tot}/dF_{\rm N}(F_{\rm N} = 0) = 0$ to be exactly obeyed in any (approximate) theory which does not minimize the total energy.

The results above assume perfectly smooth surfaces. The JKR (and DMT) theory results can, however, be applied also to surfaces with roughness assuming that the wavelength λ of the most longest (relevant) surface roughness component is much smaller than the diameter of the contact region. In that case one only needs to replace the work of adhesion $\Delta\gamma$ for flat surfaces with an effective work of adhesion $\gamma_{\rm eff}$ obtained for the rough surfaces. We will now describe how one can calculate $\gamma_{\rm eff}$.

III. THEORY: BASIC EQUATIONS

We now show how surface roughness can be taken into account in adhesive contact mechanics. We consider two limiting cases similar to the JKR and DMT theories for adhesion of a ball on a flat. The theory presented below is not based on the standard Greenwood-Williamson[10,11] picture involving contact between asperities, but on the Persson contact mechanics theory.

A. JKR-limit (review)

In the JKR-limit the spatial extent of the wall-wall interaction potential is neglected so the interaction is fully characterized by the work of adhesion $\Delta\gamma$. The contact between randomly rough surfaces in this limit was studied in Ref. 41 and here we only review the most important results.

In order for two elastic solids with rough surfaces to make adhesive contact it is necessary to deform the surfaces elastically, otherwise they would only make contact in three points and the adhesion would vanish, at least if the spatial extend of the adhesion force is neglected. Deforming the surfaces to increase the contact area A results in some interfacial bonding $-\Delta\gamma A$ (where $\Delta\gamma = \gamma_1 + \gamma_2 - \gamma_{12}$ is the change in the interfacial energy per unit area upon contact), but it costs elastic deformation energy $U_{\rm el}$, which reduces the effective binding. That is, during the removal of the block from the substrate the elastic compression energy stored at the interface is given back and helps to break the adhesive bonds in the area of real contact. Most macroscopic solids do not adhere with any measurable force, which implies that the total interfacial energy $-\Delta\gamma A + U_{\rm el}$ vanishes, or nearly vanishes, in most cases.

The contact mechanics theory of Persson[6,41–47] can be used to calculate (approximately) the stress distribution at the interface, the area of real contact, and the interfacial separation between the solid walls.[42,43] In this theory the interface is studied at different magnifications $\zeta = L/\lambda$, where L is the linear size of the system and λ the resolution. We define the wavevectors $q = 2\pi/\lambda$ and $q_0 = 2\pi/L$ so that $\zeta = q/q_0$. The theory focuses on the probability distribution $P(\sigma, \zeta)$ of stresses σ acting at the interface when the system is studied at the magnification ζ. In Ref. 42 an approximate diffusion equation of motion was derived for $P(\sigma, \zeta)$. To solve this equation one needs boundary conditions. If we assume that, when studying the system at the lowest magnification $\zeta = 1$ (where no surface roughness can be observed, i.e., the surfaces appear perfectly smooth), the stress at the interface is constant and equal to $p_{\rm N} = F_{\rm N}/A_0$, where $F_{\rm N}$ is the load and A_0 the nominal contact area, then $P(\sigma, 1) = \delta(\sigma - p_{\rm N})$. In addition to this "initial condition" we need two boundary conditions along the σ-axis. Since there can be no infinitely large stress at the interface we require $P(\sigma, \zeta) \to 0$ as $\sigma \to \infty$. For adhesive contact, which interests us here, tensile stress occurs at the interface close to the boundary lines of the contact regions. In this case we have the boundary condition $P[-\sigma_{\rm a}(\zeta), \zeta] = 0$, where $\sigma_{\rm a} > 0$ is the largest (locally averaged at magnification ζ) tensile stress possible. Hence, the detachment stress $\sigma_{\rm a}(\zeta)$ depends on the magnification and can be related to the effective interfacial energy (per unit area) $\gamma_{\rm eff}(\zeta)$ using the theory of cracks.[6] The effective interfacial binding energy

$$\gamma_{\rm eff}(\zeta)A(\zeta) = \Delta\gamma\, A(\zeta_1)\eta - U_{\rm el}(\zeta),$$

where $A(\zeta)$ denotes the (projected) contact area at the magnification ζ, and $A(\zeta_1)\eta$ is the real contact area, which is larger than the projected contact area $A(\zeta_1)$, i.e., $\eta \geq 1$ (e.g., if the rigid solid is rough and the elastic solid has a flat surface $\eta > 1$, see Ref. 41 for an expression for η). $U_{\rm el}(\zeta)$ is the elastic energy stored at the interface due to the elastic deformation of the solids on length scale shorter than $\lambda = L/\zeta$, necessary in order to bring the solids into adhesive contact.

The area of apparent contact (projected on the xy-plane) at the magnification ζ, $A(\zeta)$, normalized by the nominal contact area A_0, can be obtained from

$$\frac{A(\zeta)}{A_0} = \int_{-\sigma_{\rm a}(\zeta)}^{\infty} d\sigma\ P(\sigma, \zeta)$$

Finally, we note that the effective interfacial energy to be used in the JKR expression for the pull-off force (1) is the macroscopic effective interfacial energy corresponding to the magnification $\zeta = 1$ (here we assume that the reference length L is of order the diameter of the JKR contact region). Thus in the numerical results presented in Sec. IV we only study the area of contact $A(\zeta_1)$ and the macroscopic interfacial energy $\gamma_{\rm eff} = \gamma_{\rm eff}(1)$, which satisfies

$$\gamma_{\rm eff}A_0 = \Delta\gamma\, A(\zeta_1)\eta - U_{\rm el}(1).$$

B. DMT-limit

The DMT-limit depends on the interaction potential between the solid walls. In this section we show how this limiting case can be studied using the Persson contact mechanics theory.

Let $p_N = F_N/A_0$ be the applied pressure (which can be both positive and negative). In the DMT-limit one assumes that the elastic deformation of the solids is the same as in the absence of an adhesive interaction, except that the external load F_N is replaced with an effective load. The latter contains the contribution to the normal force from the adhesive force acting in the non-contact interfacial surface area: $F_0 = F_N + F_{ad}$. If we divide this equation by the nominal contact area A_0 we get

$$p_0 = p_N + p_{ad}.$$

The adhesive pressure

$$p_{ad} = \frac{1}{A_0}\int_{n.c.} d^2x\ p_a[u(\mathbf{x})], \tag{2}$$

where $p_a(u)$ is the interaction force per unit area when two flat surfaces are separated by the distance u. In (2) the integral is over the non-contact (n.c.) area. In this study we assume that there is a force per unit area (pressure) between the surfaces given by ($u \geq 0$, see, e.g., Fig. 2):

$$p_a = B\left[\left(\frac{d_c}{u+d_c}\right)^n - \alpha\left(\frac{d_c}{u+d_c}\right)^m\right], \tag{3}$$

where the cut-off d_c is a typical bond length and α a number, which we take to be either 0 or 1. The interaction potential between solid surfaces can have different form depending on the nature of the interaction (e.g., Coulomb interaction between charged walls, van der Waals interaction or chemical interaction), so we consider a rather general case which allow us to vary the extent of the attractive and repulsive part of the potential. van der Waals interaction correspond to $n = 3$ and is used in most of the calculations. Coulomb interaction between uniformly charged surfaces would correspond to $n = 0$. Chemical bonding is short-ranged and would qualitatively correspond to a large n ($n > 3$) but in this case an exponential interaction, $\sim\exp(-z/a)$, between the walls would be more realistic. The parameter B is determined by the work of adhesion (per unit surface area):

$$\int_0^\infty du\ p_{ad}(u) = Bd_c\frac{(m-1)-(n-1)\alpha}{(m-1)(n-1)} = \Delta\gamma,$$

so that

$$B = \frac{\Delta\gamma}{d_c}\frac{(m-1)(n-1)}{(m-1)-\alpha(n-1)}.$$

If $P(u)$ denotes the distribution of interfacial separations then we can also write (2) as

$$p_{ad} = \int_{0+}^\infty du\ p_a(u)P(u).$$

In Ref. 45 we have derived an expression for $P(u)$ using the Persson contact mechanics theory. In the numerical results presented below we have used the expression for $P(u)$ given by Eq. (17) in Ref. 45 (see also in the following).

The effective interfacial energy can in the DMT-limit be calculated using

$$\gamma_{eff} = \int_{0+}^\infty du\ \phi(u)P(u) + \Delta\gamma\frac{A}{A_0} - \frac{U_{el}}{A_0},$$

where $A = A_r$ is the (repulsive) contact area and where $\phi(u)$ is the interaction potential per unit surface area for flat surfaces separated by the distance u and given by

$$\phi(u) = \int_u^\infty du\ p_a(u).$$

Thus in the present case

$$\phi(u) = \frac{Bd_c}{n-1}\left(\frac{d_c}{u+d_c}\right)^{n-1} - \frac{Bd_c\alpha}{m-1}\left(\frac{d_c}{u+d_c}\right)^{m-1}.$$

For $u = 0$ an infinite hard wall occurs and we define the (repulsive) contact area A_r when the surface separation $u = 0$. In the calculations below we use $n = 3$ and $m = 9$ and $\alpha = 0$ (Sec. IV) and $\alpha = 1$ (Sec. V). The interaction pressure for these two cases are shown in Fig. 2.

The probability distribution of interfacial separations $P(u)$ can be calculated as follows: We define $u_1(\zeta)$ to be the (average) height separating the surfaces which appear to come into contact when the magnification decreases from ζ to $\zeta - \Delta\zeta$, where $\Delta\zeta$ is a small (infinitesimal) change in the magnification. $u_1(\zeta)$ is a monotonically decreasing function of ζ, and can be calculated from the average interfacial separation $\bar{u}(\zeta)$ and the contact area $A(\zeta)$ using (see Ref. 44)

$$u_1(\zeta) = \bar{u}(\zeta) + \bar{u}'(\zeta)A(\zeta)/A'(\zeta).$$

The equation for the average interfacial separation $\bar{u}(\zeta)$ is given in Ref. 44. The (apparent) relative contact area $A(\zeta)/A_0$ at the magnification ζ is given by

$$\frac{A(\zeta)}{A_0} = \mathrm{erf}\left[\frac{p_0}{2G(\zeta)^{1/2}}\right],$$

where

$$G(\zeta) = \frac{\pi}{4}\left(\frac{E}{1-\nu^2}\right)^2\int_{q_0}^{\zeta q_0} dq q^3 C(q),$$

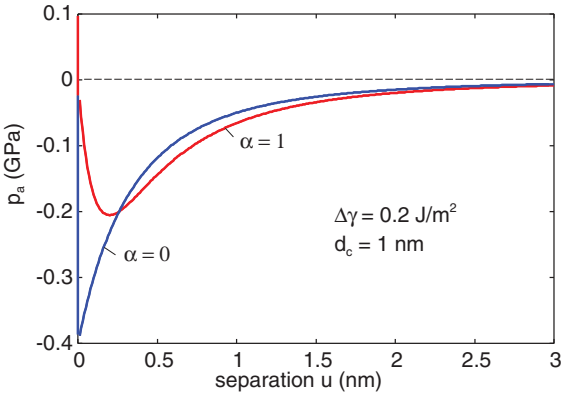

FIG. 2. The adhesive pressure for $n = 3$ and $m = 9$ and $\alpha = 1$ (red line) and $\alpha = 0$ (blue line). In the calculation we assumed $\Delta\gamma = 0.2$ J/m^2 and $d_c = 1$ nm.

where $C(q)$ is the surface roughness power spectrum. In what follows we will denote this contact area as the *repulsive* contact area A_r since the normal stress is repulsive within this area, unless otherwise stated. We also define an *attractive* contact area A_a as the surface area where the surface separation $0 < u < d_c$; in this surface separation interval the wall-wall interaction is attractive. The cut-off length d_c is quite arbitrary and in Ref. 18 another cut-off length (of order d_c) was used to define the attractive contact area.

The probability distribution $P(u)$ can be written as[45]

$$P(u) \approx \frac{1}{A_0}\int d\zeta\ [-A'(\zeta)]\frac{1}{\left(2\pi h^2_{\rm rms}(\zeta)\right)^{1/2}} \times\left[\exp\left(-\frac{(u-u_1(\zeta))^2}{2h^2_{\rm rms}(\zeta)}\right)+\exp\left(-\frac{(u+u_1(\zeta))^2}{2h^2_{\rm rms}(\zeta)}\right)\right],$$

where $h^2_{\rm rms}(\zeta)$ is the mean of the square of the surface roughness amplitude including only roughness components with the wavevector $q > q_0\zeta$, and given by

$$h^2_{\rm rms}(\zeta) = \int_{q>q_0\zeta} d^2q\ C(q).$$

C. Scale-dependent Tabor length $d_T(q)$

The contact between surfaces with roughness on many length scales involves contact between asperities with many different radii of curvature. Thus at low magnifications we only observe long-wavelength roughness and the asperity radius of curvature may be macroscopic, e.g., ∼1 mm or more. At high magnification, nanoscale roughness will be observed involving asperities which may have radius of curvature in the nm range. Thus adhesion at long length scale may appear JKR-like while at short enough length scale the adhesion may appear DMT-like. One can define a magnification or length-scale dependent Tabor length $d_T(\zeta)$ ($\zeta = q/q_0$), in the following way: If we include only roughness components with wavevector $q < \zeta q_0$ the mean summit asperity curvature is[48]

$$\frac{1}{R^2(\zeta)} = \frac{16}{3\pi}\int_{q_0}^{\zeta q_0} dq\ q^5 C(q).$$

We define

$$d_T(\zeta) = \left(\frac{R(\zeta)[\gamma_{\rm eff}(\zeta)]^2}{E_r^2}\right)^{1/3}.$$

If $d_T(\zeta) \ll d_c$ the contact at the magnification $\zeta = q/q_0$, will appear DMT-like while if $d_T(\zeta) \gg d_c$ the contact will appear JKR-like. In what follows we will sometimes denote $d_T(\zeta)$ with $d_T(q)$ ($q = \zeta q_0$).

IV. THEORY: NUMERICAL RESULTS

We now present numerical results which illustrate the two adhesion theories presented above. The JKR-like theory has been studied before (see Ref. 41) so we focus mainly on the DMT-like theory. In the calculations we vary $\Delta\gamma$ and n, but we always use the cut-off $d_c = 0.4$ nm and $\alpha = 0$ unless otherwise stated.

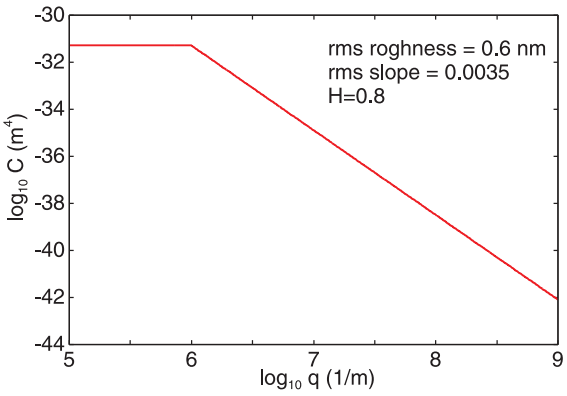

FIG. 3. The surface roughness power spectrum $C(q)$ as a function of the wavevector q ($\log_{10} - \log_{10}$ scale), used in the present calculations. The power spectrum corresponds to a surface with the rms roughness amplitude 0.6 nm, the rms slope 0.0035 and the Hurst exponent $H = 0.8$.

A. Surface roughness power spectrum $C(q)$ and Tabor length $d_T(q)$

In Fig. 3 we show the surface roughness power spectrum $C(q)$ (PSD) as a function of the wavevector q ($\log_{10} - \log_{10}$ scale), used in the present calculations. The power spectrum corresponds to a surface with the rms roughness amplitude 0.6 nm, the rms slope 0.0035 and the Hurst exponent $H = 0.8$. Fig. 4 shows the surface topography of one realization of a randomly rough surface with the surface roughness power spectrum shown in Fig. 3. The difference between the lowest and highest point is about 5 nm, i.e., about 10 times higher than the rms roughness 0.6 nm.

In the calculations below we use the Young's modulus $E = 10^{12}$ Pa, Poisson ration $\nu = 0.5$ and the work of adhesion $\Delta\gamma = 0.1$–0.4 J/m^2. Figure 5 shows the Tabor length parameter d_T as a function of the wavevector ($\log_{10} - \log_{10}$ scale), for $\Delta\gamma = 0.3$ J/m^2. Note that the contact mechanics is DMT-like for short length scales (or large wavevectors) with $d_T < d_c = 0.4$ nm, while it is JKR-like for long length scales (small wavevectors).

B. Results for different work of adhesion $\Delta\gamma$

Fig. 6 shows the normalized (projected) area of contact A/A_0 and the effective interfacial energy $\gamma_{\rm eff} = [E_{\rm ad} - U_{\rm el}]/A_0$ [where $E_{\rm ad}$ is the (attractive) van der Waals interaction energy and $U_{\rm el}$ the (repulsive) elastic deformation energy] as a function of the nominal applied pressure p_N acting on the block.

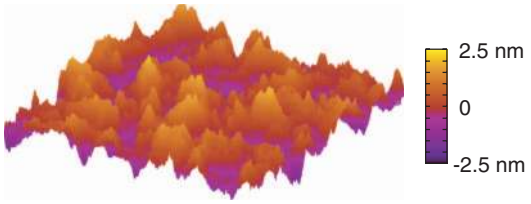

FIG. 4. Surface topography of one realization of a surface with the surface roughness power spectrum shown in Fig. 3. The difference between the lowest and highest point is about 5 nm, i.e., about 10 times higher than the rms roughness 0.6 nm (see Appendix A in Ref. 6).

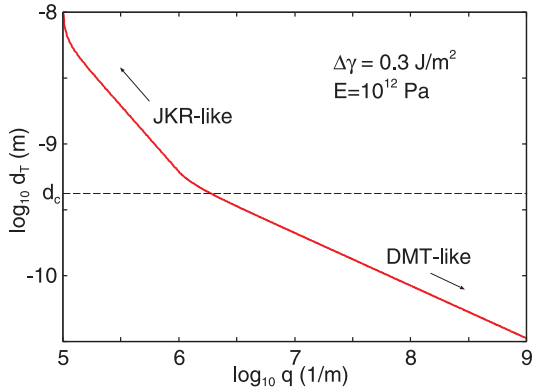

FIG. 5. The Tabor length parameter d_T as a function of the wavevector ($\log_{10}$ − $\log_{10}$ scale). For the surface with the power spectrum given in Fig. 3 and with the elastic modulus $E = 10^{12}$ Pa ($\nu = 0.5$) and work of adhesion $\Delta\gamma = 0.3$ J/m^2.

In the DMT-like theory (red curve) $A = A_r$ is the repulsive contact area while in the JKR-like theory (blue curves) A is the total contact area (which has both an attractive and a repulsive part). Results are shown for the work of adhesion $\Delta\gamma = 0.0$ (green curve), 0.1, 0.2, 0.3, and 0.4 J/m^2. The red and blue lines correspond to DMT-like and JKR-like approximations, respectively. Note that the area of contact at zero pressure is about a factor 3 larger in the JKR-like approximation as compared to the DMT-like approximation. This is consistent with the results for adhesion of sphere on flat (see Sec. II) where the JKR theory predict about 2 times larger contact area than the DMT theory. On the other hand, Fig. 6(b) shows that the effective interfacial binding energies are similar, which is also consistent with the results of Sec. II. The effective work of adhesion to be used in macroscopic adhesion applications, i.e., the pull-off of a ball from a flat (Sec. II) is γ_{eff} for the applied pressure $p_N = 0$, and in all cases in Fig. 6 $\gamma_{eff}(p_N = 0)$ is less than half of the work of adhesion $\Delta\gamma$ for smooth surfaces.

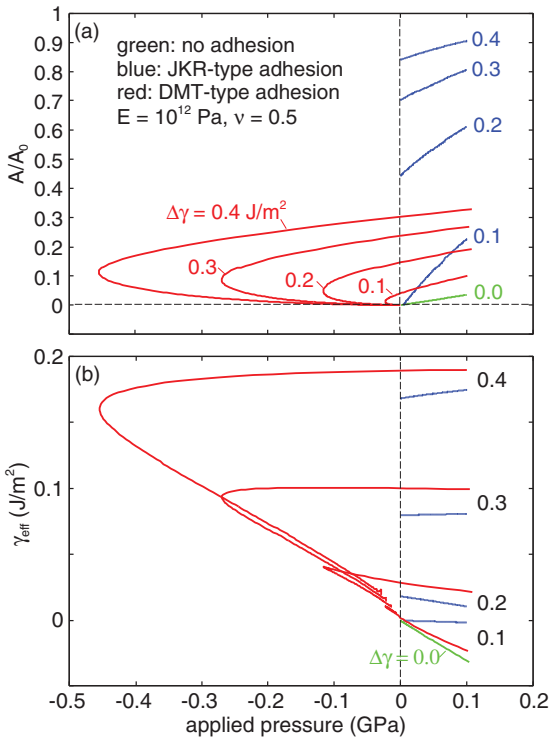

FIG. 6. (a) The normalized (projected) area of contact A/A_0 and (b) the effective interfacial energy $\gamma_{eff} = [E_{ad} - U_{el}]/A_0$ [where E_{ad} is the (attractive) van der Waals interaction energy and U_{el} the (repulsive) elastic deformation energy] as a function of the applied (nominal) pressure p_N acting on the block. In the DMT-like theory (red curve) $A = A_r$ is the repulsive contact area while in the JKR-like theory (blue curves) A is the total contact area (which has both an attractive and a repulsive part). Results are shown for the work of adhesion $\Delta\gamma = 0.0$ (green curve), 0.1, 0.2, 0.3, and 0.4 J/m^2. The red and blue lines correspond to DMT-like and JKR-like approximations, respectively. The elastic solid Young's modulus $E = 10^{12}$ Pa and Poisson number $\nu = 0.5$.

Fig. 6(b) shows that for $\Delta\gamma = 0.1$ J/m^2 in the JKR-limit the effective interfacial binding energy, and hence also the pull-off force, vanish. Nevertheless, Fig. 6(a) shows that in the JKR-limit the contact area as a function of p_N increases much faster with increasing p_N than in the absence of adhesion (green line), i.e., even if no adhesion manifests itself during pull-off, the contact area and hence other properties such as the friction force, may be strongly enhanced by the adhesive interaction. In the DMT-limit the effective interfacial binding energy is always non-zero if the wall-wall interaction does not vanish beyond some fix wall-wall separation. This is easy to understand since when the wall-wall separation is larger than the highest asperity the solid walls will only interact with the long-ranged attractive wall-wall potential and increasing the separation to infinity will always require a finite amount of work making $\gamma_{eff}(p_N = 0)$ always non-zero in the DMT-limit.

Let us now discuss the slopes (with increasing p_N) of the $\gamma_{eff}(p_N)$ curves in Fig. 6(b) for $p_N = 0$. As pointed out in Sec. II, in an exact treatment, as a function of the external load p_N the total energy $-A_0\gamma_{eff} = -E_{ad} + U_{el}$ must have a minimum at $p_N = 0$. However, the theories described above are not exact, and are not based on a treatment which minimize the total energy, but rather focus on the force (or stress) (in the DMT-like model) or on a combined energy and stress treatment (in the JKR-like model). This is the reason for why the slope of the $\gamma_{eff}(p_N)$ curves for large $\Delta\gamma$ is positive rather than negative. However, the slope is rather small compared to the (absolute value of) the slope for the non-adhesive interaction (green curve). In addition, the surface we use has a Tabor length with $d_T(q) \ll d_c$ for large q and $d_T(q) \gg d_c$ for small q so strictly speaking neither the JKR-limit or the DMT-limit is correct or valid. For other surfaces which have $d_T(q) \ll d_c$ or $d_T(q) \gg d_c$ for all q, the JKR-like and DMT-like theories may be more accurate and the slope of the $\gamma_{eff}(p_N)$ curve negative.

Fig. 7 shows the applied pressure as a function of the average separation for the work of adhesion $\Delta\gamma = 0.0$ (green curve), 0.1, 0.2, 0.3, and 0.4 J/m^2. The blue dashed curve is the van der Waals interaction force per unit area $p_a = B[d_c/(u + d_c)]^3$, where $d = 0.4$ nm and u the distance from the hard wall. The parameter B is chosen to reproduce the given work of adhesion for flat surfaces. Note that the attractive interaction between the walls is already strong at distances where negligible wall-wall interaction would occur (as described by the blue dashed line). This is of course due to adhesive interaction involving high asperities, which prevails even when the

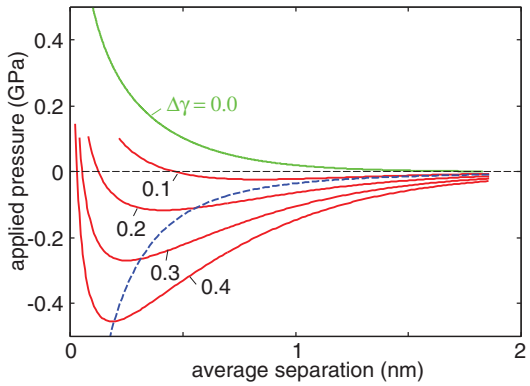

FIG. 7. The applied pressure as a function of the average separation for the work of adhesion $\Delta\gamma = 0.0$ (green curve), 0.1, 0.2, 0.3, and 0.4 J/m^2. The blue dashed curve is the van der Waals interaction force per unit area $p_a = B[d_c/(u + d_c)]^3$, where $d_c = 0.4$ nm and u the distance from the hard wall. The parameter B is chosen to reproduce the given work of adhesion for flat surfaces.

average wall-wall separation is relatively large. For the case of no adhesion (green curve) the wall-wall interaction is purely repulsive as the asperities get compressed on decreasing the wall-wall separation. Asymptotically (large separation) this repulsive interaction is exponential $p_N \sim \exp(-u/u_0)$ where the reference length u_0 is of order the rms surface roughness.

C. Results for different interaction potential exponent *n* and factor *α*

Fig. 8 shows the normalized (projected) repulsive area of contact A_r/A_0 and the effective interfacial energy $\gamma_{eff} = [E_{ad} - U_{el}]/A_0$ [where E_{ad} is the (attractive) van der Waals interaction energy and U_{el} the (repulsive) elastic deformation energy] as a function of the nominal pressure acting on the block. Results are shown for the work of adhesion $\Delta\gamma = 0.3$ J/m^2 and the interaction force index $n = 1.5$, 2, 3, and 4 ($p_a = B[d_c/(u + d_c)]^n$, i.e., $\alpha = 0$). The results are for the DMT-like approximation. The elastic solid Young's modulus $E = 10^{12}$ Pa and Poisson number $\nu = 0.5$.

Fig. 8 shows that as the interaction becomes more short ranged (n increases from 1.5 to 4) (at fixed work of adhesion $\Delta\gamma$) the contact area increases while the effective interfacial binding energy γ_{eff} decreases. The latter is easy to understand: in the limiting case when $n \to 0$ the interaction potential has infinite extend (and infinitesimal strength in such a way that the work of adhesion $\Delta\gamma = 0.3$ J/m^2) and in this case γ_{eff} must equal $\Delta\gamma$. At the same time due to the weak (infinitesimal) force the contact area at the load $p_N = 0$ must vanish, which explains the behaviour observed in Fig. 8(a).

Fig. 9 shows the applied pressure as a function of the average separation for the work of adhesion $\Delta\gamma = 0.3$ J/m^2 and the interaction force index $n = 1.5$, 2, 3, and 4 ($p_a = B[d_c/(u + d_c)]^n$). The results are for the DMT-like approximation. Note that when n decreases the more long-range the effective attraction but at the same time the smaller the maximal attraction, which again reflects that $\Delta\gamma$ is kept fixed.

All the numerical results presented above were for the cut-off length $d_c = 0.4$ nm and the repulsion factor $\alpha = 0$. We now consider the case $\alpha = 1$ with $m = 9$ (and $n = 3$). We also

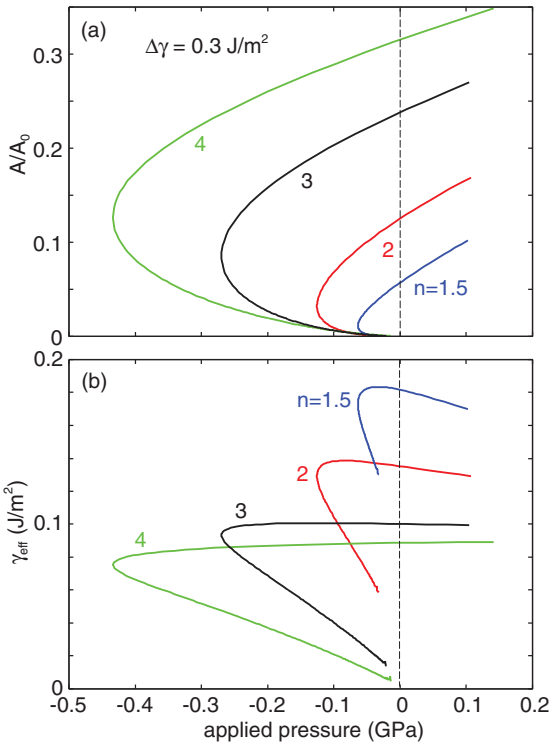

FIG. 8. (a) The normalized (projected) repulsive area of contact A_r/A_0 and (b) the effective interfacial energy $\gamma_{eff} = [E_{ad} - U_{el}]/A_0$ [where E_{ad} is the (attractive) van der Waals interaction energy and U_{el} the (repulsive) elastic deformation energy] as a function of the nominal pressure p_N acting on the block. Results are shown for the work of adhesion $\Delta\gamma = 0.3$ J/m^2 and the interaction force index $n = 1.5$, 2, 3, and 4 ($p_a = B[d_c/(u + d_c)]^n$). From the DMT-like approximation (see text). The elastic solid Young's modulus $E = 10^{12}$ Pa and Poisson number $\nu = 0.5$.

use $d_c = 1.0$ nm. These are the same parameters we will use when comparing the theory with exact numerical simulation results in Sec. V. We consider a surface with the rms roughness 0.5 nm, the roll-off wavevector $q_r = 1.0 \times 10^6$ m^{-1} and the small and large wavevector cut-off $q_0 = 2.5 \times 10^5$ m^{-1} and $q_1 = 3.2 \times 10^7$ m^{-1}.

Fig. 10 shows the normalized (projected) repulsive contact area A_r/A_0 as a function of the nominal pressure p_N acting

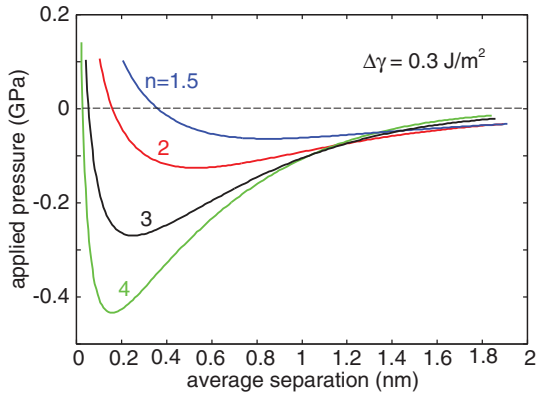

FIG. 9. The applied pressure p_N as a function of the average separation for the work of adhesion $\Delta\gamma = 0.3$ J/m^2 and the interaction force index $n = 1.5$, 2, 3, and 4 ($p_a = B[d_c/(u + d_c)]^n$). From the DMT-like approximation (see text).

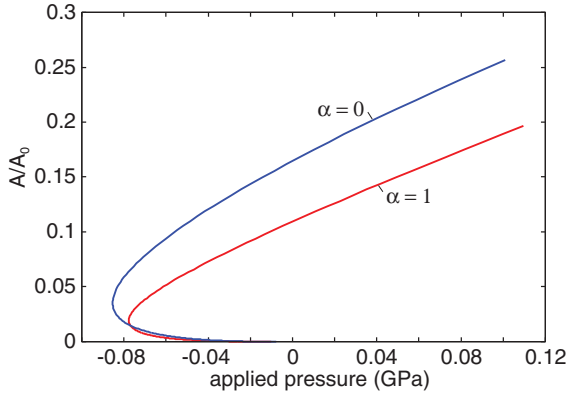

FIG. 10. The normalized (projected) repulsive area of contact A_r/A_0 as a function of the nominal pressure p_N acting on the block. Results are shown for the work of adhesion $\Delta\gamma = 0.2$ J/m^2 and the interaction index $n = 3$ and $m = 9$ and with $d_c = 1$ nm. Blue curve is with $\alpha = 0$ and red curve with $\alpha = 1$. From the DMT-like approximation (see text).

on the block. Results are shown for the work of adhesion $\Delta\gamma = 0.2$ J/m^2. The blue curve is with $\alpha = 0$ and red curve with $\alpha = 1$.

Fig. 11 shows the applied pressure p_N as a function of the average surface separation for the work of adhesion $\Delta\gamma = 0.2$ J/m^2. Again the blue curve is with $\alpha = 0$ and red curve with $\alpha = 1$.

V. COMPARISON OF THE DMT-LIKE THEORY WITH EXACT ANALYTICAL RESULTS

In this section we use the interaction potential (3) with $n = 3$, $m = 9$, and $\alpha = 1$ with $d_c = 1$ nm (see Fig. 2 and the Appendix). The power spectral density adopted in the numerical calculations (see the Appendix for the summary of the numerical simulation model) is shown in Fig. 12.

In Figs. 13–15 we show, respectively, the normalized and projected area of repulsive contact A_r/A_0, of attractive contact A_a/A_0 and the total interaction area $A/A_0 = (A_r + A_a)/A_0$ as a function of the applied (nominal) pressure p_N. Red dots are from the (deterministic) simulations, whereas black solid

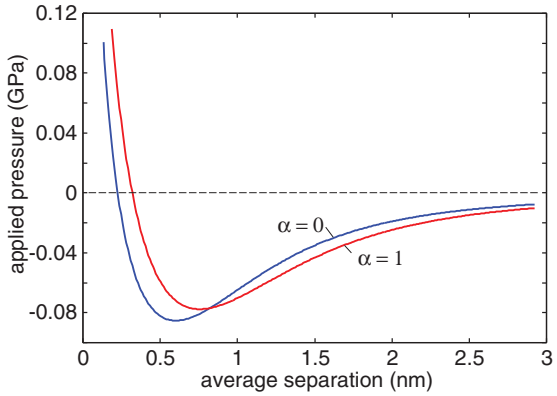

FIG. 11. The applied pressure p_N as a function of the average separation for the work of adhesion $\Delta\gamma = 0.2$ J/m^2 and the interaction index $n = 3$ and $m = 9$ and with $d_c = 1$ nm. Blue curve is with $\alpha = 0$ and red curve with $\alpha = 1$. From the DMT-like approximation (see text).

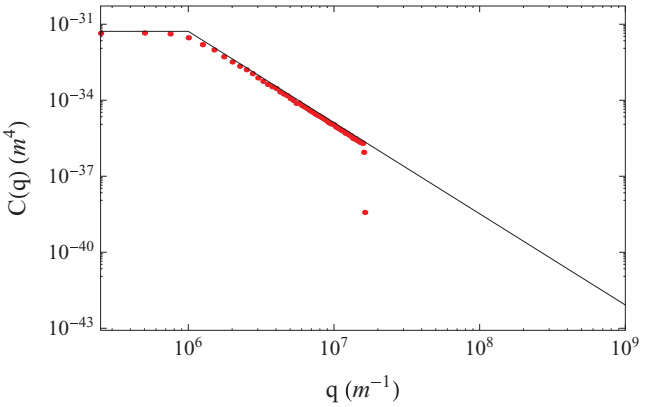

FIG. 12. Solid line: Power spectral density $C(q)$ as a function of q. For an isotropic surface roughness with cut-off frequency $q_0 = q_r/4$, root-mean-square roughness $h_{rms} = 0.6$ nm, and with self-affine regime in the frequency range $q_r = 10^6$ m^{-1} to $q_1 = 10^3 q_r$. The Hurst exponent is $H = 0.8$. Dotted line: The PSD adopted in the numerical calculations is truncated at $q_1 = 64q_0$, with 8 divisions at the smallest length scale (q_1), resulting in a $h_{rms} = 0.52$ nm and mean square slope 0.00115.

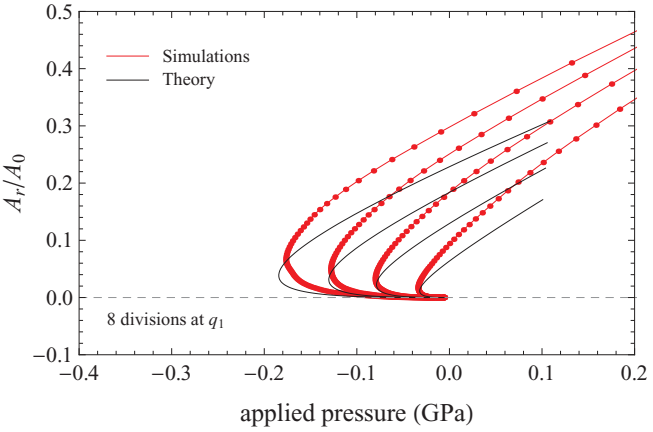

FIG. 13. Normalized (projected) area of repulsive contact A_r/A_0 as a function of the applied pressure p_N, for different values of work of adhesion $\Delta\gamma = 0.1,\ 0.2,\ 0.3,\ 0.4$ J/m^2. For an elastic solid with $E_r = 1.33 \times 10^{12}$ GPa and for the surface roughness of Fig. 12.

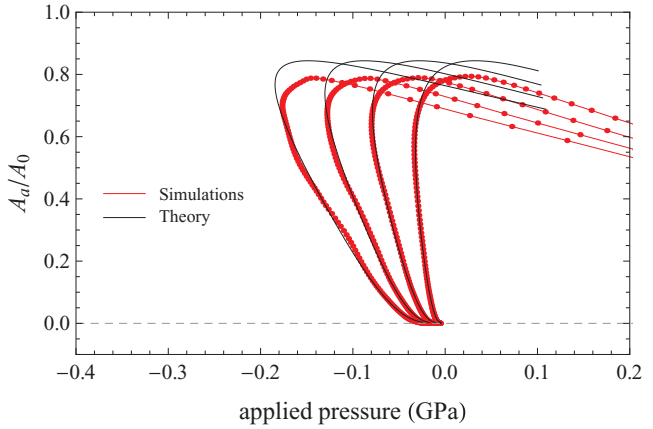

FIG. 14. Normalized (projected) area of attractive contact A_a/A_0 as a function of the applied pressure p_N, for different values of work of adhesion. For the same parameters as in Fig. 13.

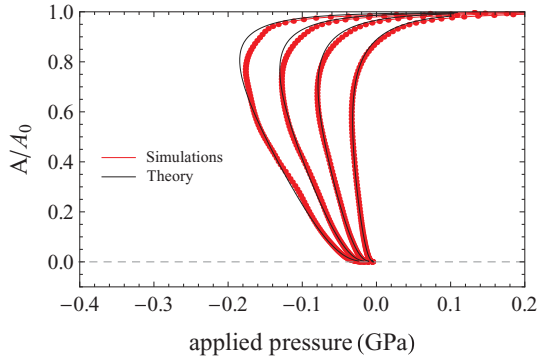

FIG. 15. Normalized (projected) contact area $A/A_0 = (A_r + A_a)$ as a function of the applied pressure p_N, for different values of work of adhesion. For the same parameters as in Fig. 13.

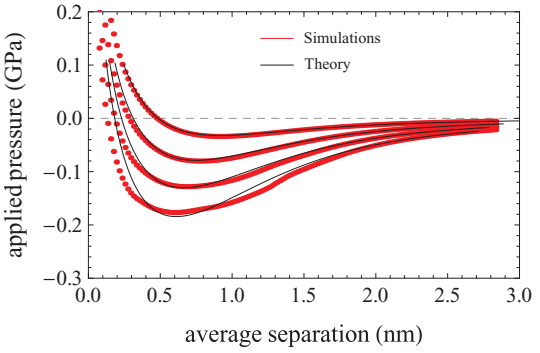

FIG. 17. Nominal pressure p_N as a function of the average interfacial separation $\bar{u}$. For the same parameters as in Fig. 13.

lines are from the mean field theory. We note that while the repulsive interaction area is slightly underestimated by the theory, the pull-off pressures are remarkably accurately captured at the different adopted values of work of adhesion. Moreover, the total interaction area (see Fig. 15), as a function of applied pressure, seems to be only marginally affected by the exact contact boundary conditions adopted in the mean field theory, resulting in a perfect match with the numerical simulation predictions, as it could have been expected. It is indeed well known that Persson contact mechanics accurately predicts the distribution of interfacial separations.[17,45] Hence the total interaction area, which is evaluated from the distribution of interfacial separation, is accurately captured too. Also note that the simulated contact is close to the DMT-limit, as shown in Fig. 16, where the repulsive area is reported as a function of the nominal repulsive pressure ($p_0 = p_N + p_{ad}$).

In Fig. 17 we show the applied pressure p_N as a function of the average interfacial separation $\bar{u}$, for different values of $\Delta\gamma$, as determined from the theory (black curves) and the numerical model. As expected from the previous arguments, the agreement is remarkably good in almost the entire range of average interfacial separations.

We stress that the power spectral density can be nowadays routinely obtained with commonly available lab profilometers. However, usually one has to adopt different acquisition techniques depending on the range of roughness length scales needed to be investigated. Therefore, it would be particularly interesting to appreciate the extent to which the macroscopic adhesive characteristics, such as pull-off pressure, depends on the effect of adding (or, inversely, not measuring) an increasing number of surface roughness frequency components. To do so, we gradually extend the numerically calculated roughness spectral components of Fig. 12, as shown in Fig. 18, up to a system size of 2^{24} mesh points. In Figs. 19–21 we show, respectively, the normalized and projected area of repulsive contact A_r/A_0, the attractive contact A_a/A_0, and the total interaction area $A/A_0 = (A_r + A_a)/A_0$ as a function of the applied nominal pressure p_N, for different truncation wavevectors. Red dots are the predictions of the simulations, whereas black solid lines are from the mean field theory. The pull-off pressure is almost independent of the large-wavevector content of the PSD, whereas the repulsive contact area, as expected, decreases by including large-wavevector (small wavelength) roughness. Moreover, the large-wavevector roughness does not contribute significantly to the h_{rms}, as is clear both theoretically and numerically from Fig. 22, where the applied pressure is reported as a function of the average interfacial separation.

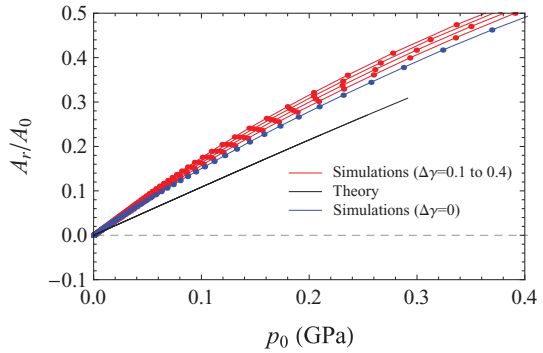

FIG. 16. Normalized (projected) repulsive area $A_r/A_0 =$ as a function of the nominal repulsive pressure $p_0 = p_N + p_{ad}$, for different values of work of adhesion. For the same parameters as in Fig. 13.

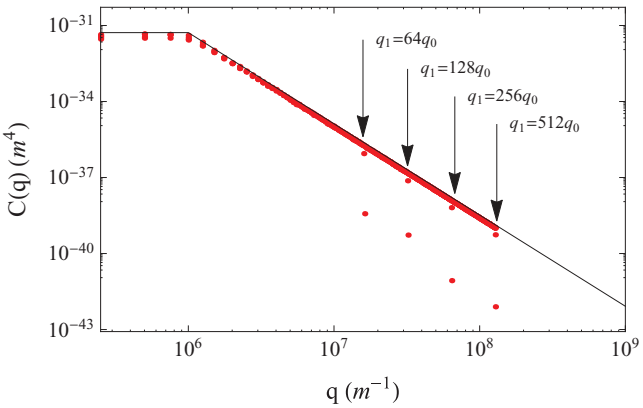

FIG. 18. Power spectral density $C(q)$ as a function of q (solid black line). For an isotropic surface roughness with cut-off $q_0 = q_r/4$ and root-mean-square roughness $h_{rms} = 0.6$ nm, and with self-affine regime in the frequency range $q_r = 10^6$ m^{-1} to $q_1 = 10^3 q_r$ ($H = 0.8$). The numerical adopted PSD (red dots) is truncated at $q_1 = [64, 128, 256, 512]q_0$, with 8 divisions at the smallest length scale (q_1).

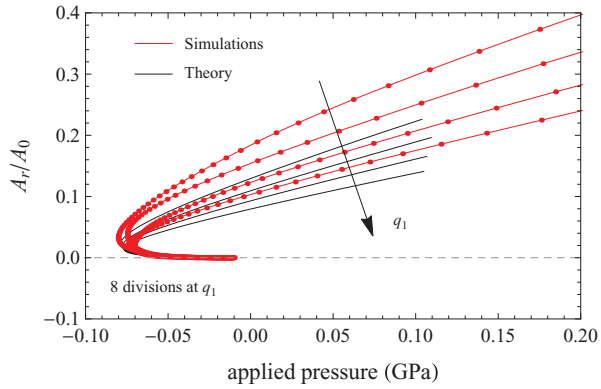

FIG. 19. Normalized (projected) area of repulsive contact A_r/A_0 as a function of the applied pressure p_N, and for $\Delta\gamma = 0.2\,J/m^2$. For an elastic solid with $E_r = 1.33 \times 10^{12}$ GPa and for the surface roughness of Fig. 18 (with $q_0 = 2.5\,10^5\ m^{-1}$, $q_r = 4q_0$, $H = 0.8$, resulting in $C_0 = 5.24 \times 10^{-32}\ m^4$), at different truncation frequencies $q_1 = 64, 128, 256, 512\,q_0$.

Finally, let us compare the theoretical predictions with simulation results for the effective interfacial energy γ_{eff}. In Fig. 23 we show the effective interfacial energy $\gamma_{eff} = [E_{ad} - U_{el}]/A_0$ [where E_{ad} is the (attractive) van der Waals interaction energy and U_{el} the (repulsive) elastic deformation energy] as a function of the nominal pressure p_N acting on the block. Results are shown for the work of adhesion $\Delta\gamma = 0.1$, 0.2, 0.3, and $0.4\,J/m^2$. The red data points are from the exact numerical simulation and the black lines from the DMT-like theory (Sec. III B) also shown in Fig. 6. The elastic solid Young's modulus $E = 10^{12}$ Pa and Poisson number $\nu = 0.5$.

In Fig. 24 we show similar results for the effective interfacial energy γ_{eff} but now for $\Delta\gamma = 0.2\,J/m^2$, and for several large wavevector cut-off $q_1 = 64q_0$, $128q_0$, and $256q_0$. Note that the effective interfacial energy γ_{eff} is rather insensitive to the large wavevector cut-off q_1. The reason for this is that the repulsive elastic energy U_{el} is dominated by the long-wavelength roughness. In both Figures 23 and 24 there is remarkable good agreement between theory and simulations.

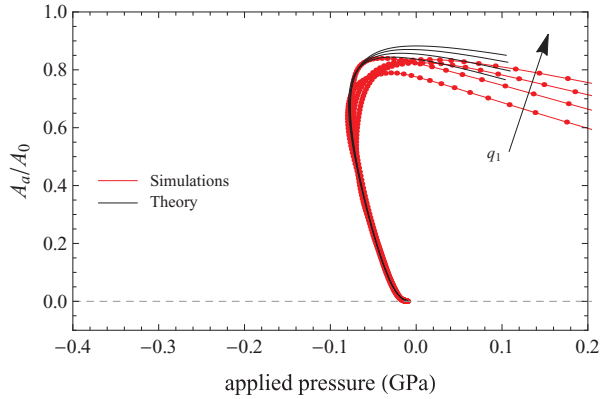

FIG. 20. Normalized (projected) area of attractive contact A_a/A_0 as a function of the applied pressure p_N. For the same parameters as in Fig. 19.

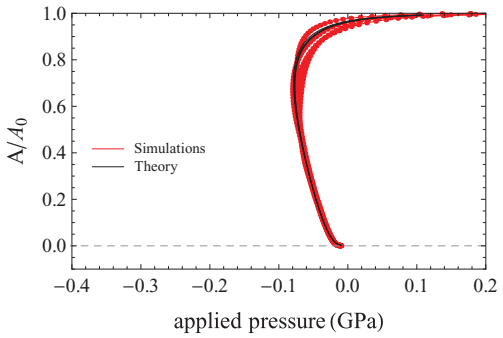

FIG. 21. Normalized (projected) contact area $A/A_0 = (A_r + A_a)$ as a function of the applied pressure p_N. For the same parameters as in Fig. 19.

VI. DISCUSSION

In the discussion above we have neglected adhesion hysteresis. Adhesion hysteresis is particularly important for viscoelastic solids such as most rubber compounds. However, even for elastic solids adhesion hysteresis may occur. Thus, not all the stored elastic energy U_{el} may be used to break adhesive bonds during pull-off but some fraction of it may be radiated as elastic waves (phonons) into the solids. This would result in an increase in the effective interfacial binding energy during pull-off, and would result in adhesion hysteresis.

We note that adhesion hysteresis is observed already for smooth surfaces in the JKR-limit (elastically soft solids) but not in the DMT-limit (hard solids).[49] Since for randomly rough surfaces the contact mechanics may be close to the DMT-limit for short length scales (high resolution) while close to the JKR-limit at large enough length scales, as in Fig. 5, one expects in many cases that the bond-breaking process involved at short length scale is reversible (no hysteresis), while the elastic deformations at large enough length scales show hysteresis, involving rapid (dissipative) processes during pull-off.

Contact mechanics for randomly rough surfaces is a hard problem to treat by numerical simulations in the JKR-limit (see the Appendix) and most published studies are close to the DMT-limit (however, see Ref. 19 for results in the JKR-limit). While this case may be relevant for many hard materials, most adhesion experiments involve soft materials like silicon rubber (PDMS). In this case the adhesion will be JKR-like in a large range of length scales.

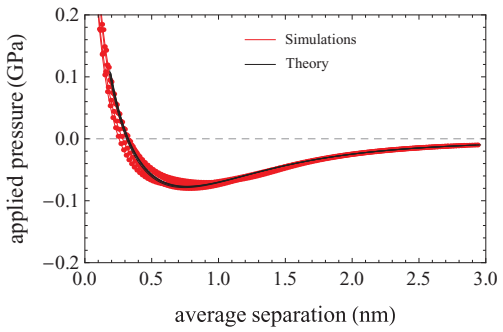

FIG. 22. Applied pressure p_N as a function of the average interfacial separation $\bar{u}$. For the same parameters as in Fig. 19.

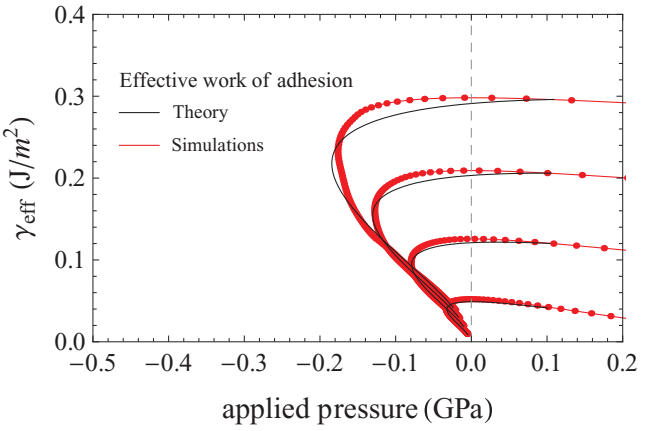

FIG. 23. The effective interfacial energy $\gamma_{\rm eff} = [E_{\rm ad} - U_{\rm el}]/A_0$ [where $E_{\rm ad}$ is the (attractive) van der Waals interaction energy and $U_{\rm el}$ the (repulsive) elastic deformation energy] as a function of the applied pressure $p_{\rm N}$ acting on the block. Results are shown for the work of adhesion $\Delta\gamma = 0.1, 0.2, 0.3$, and 0.4 J/m^2. The red data points are from the exact numerical simulation and the black lines from the DMT-like theory (Sec. III B) also shown in Fig. 6. For the same parameters as in Fig. 13.

We note that adhesion problems which are JKR-like for large length scales and DMT-like for short length scales can be approximately treated using the theory presented above: We plot the Tabor length $d_{\rm T}(q)$ as a function of log$q$ as in Fig. 5 and divide the log$q$ axis into a large wavevector region $q > q^*$ and a short wavevector region $q < q^*$ where $d_{\rm T}(q^*) = d_{\rm c}$. We use the DMT-like theory to calculate $\gamma_{\rm eff}(q^*)$ including only the roughness components with $q > q^*$. Next, we apply the JKR-like theory for the $q < q^*$ region with $\Delta\gamma = \gamma_{\rm eff}(q^*)$. This treatment is of course only approximate since there will be a region close to $q = q^*$ which is neither DMT-like nor JKR-like, but if this region (on the log$q$-scale) is small compared to the total decades of length scales involved it may constitute a good approximation. This picture of adhesion is similar to the Renormalization Group (RG) procedure used in statistical physics where short wavelength degrees of freedom (here the short wavelength roughness involved in the DMT-like contact mechanics) are integrated out (removed) to obtain effective equations relevant at the macroscopic length scale (here the JKR-like contact mechanics). When applying the RG procedure one often finds that processes or phenomena which appear very different at the microscopic (say atomistic) limit result in the same macroscopic equations of motion, e.g., the Navier-Stokes equations of fluid flow does not really depend on the exact nature of the force law between the atoms or molecules except it determines or influence the fluid density and viscosity. Similar, for large surface roughness the force law between the surfaces, which is important at short length scale (DMT-limit) does not really matter for the macroscopic (JKR-like) contact mechanics except it determines the effective interfacial binding energy $\Delta\gamma = \gamma_{\rm eff}(q^*)$ to be used in the JKR theory. This statement does not hold when the surface roughness amplitude is very small, such as in the present study, because the (average) surface separation in the non-contact area is only of order ∼1 nm and at this separation the wall-wall interaction potential is still important, in particular, for small index n. For charged bodies, due to the long range of the coulomb interaction, the wall-wall interaction potential is important for any wall-wall separation.

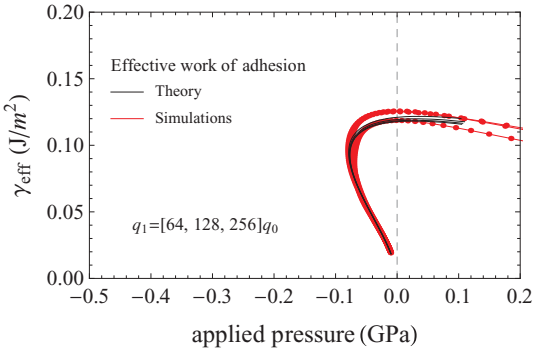

FIG. 24. The effective interfacial energy $\gamma_{\rm eff} = [E_{\rm ad} - U_{\rm el}]/A_0$ [where $E_{\rm ad}$ is the (attractive) van der Waals interaction energy and $U_{\rm el}$ the (repulsive) elastic deformation energy] as a function of the applied pressure $p_{\rm N}$ acting on the block. Results are shown for the large wavevector cut-off $q_1 = 64q_0$, $128q_0$, and $256q_0$. For the work of adhesion $\Delta\gamma = 0.2$ J/m^2. The red data points are from the exact numerical simulation and the black lines from the DMT-like theory (Sec. III B). For the same parameters as in Fig. 19.

VII. CONCLUSIONS

We have discussed how surface roughness influences the adhesion between elastic solids. We have introduced a Tabor number which depends on the length scale or magnification, and which gives information about the nature of the adhesion at different length scales. In most cases the contact mechanics will be DMT-like at short length scales and JKR-like at large length scales. We have considered two limiting cases relevant for (a) elastically hard solids with weak adhesive interaction (DMT-limit) and (b) elastically soft solids or strong adhesive interaction (JKR-limit). For the former cases we have studied the nature of the adhesion using different adhesive force laws ($F \sim u^{-n}$, $n = 1.5$–4, where u is the wall-wall separation). The theory results have been compared to the results of exact numerical simulations, and good agreement between theory and the simulation results was obtained.

ACKNOWLEDGMENTS

M.S. acknowledges FZJ for the support and the kind hospitality received during his visit to the PGI-1, where this work has been performed. M.S. also acknowledges COST Action MP1303 for grant (Grant No. STSM-MP1303-090314-042252) and support from MultiscaleConsulting. We thank M.H. Müser for useful discussions and comments on the manuscript.

APPENDIX: NUMERICAL MODEL

We consider the case of two elastic solids patterned with random or deterministic roughness. We assume the generic roughness to be characterized by a small wavelength cut-off $q_0 = 2\pi/L_0$ with $L_0 \ll L$, where L is the representative size of the macroscopic contact region between the two solids. Given such a large difference of length scales, we can easily identify a representative elementary volume (RVE) of interface of length scale $L_{\rm RVE}$, with $L_0 \ll L_{\rm RVE} \ll L$, over which we can average out the contact mechanics occurring at smaller length scales (say, at $\lambda \ll L_{\rm RVE}$). Note that the numerical or

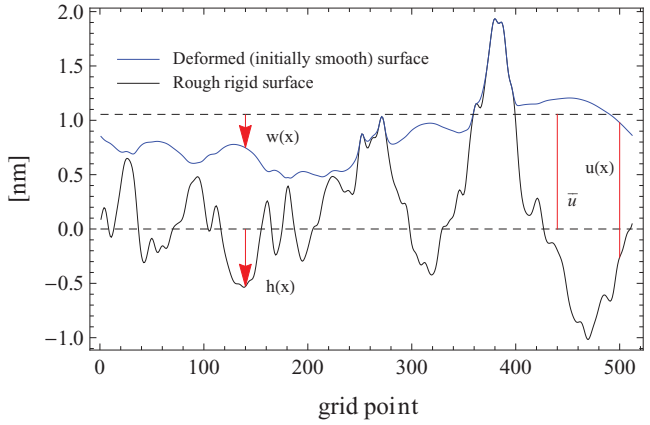

FIG. 25. Description of the gap [see Eq. (A1)] resulting from a generic cross section of the contact interface. By close inspection of the figure, it is easily agreeable that the deformed profile for an adhesive interaction qualitatively differs from the adhesiveless case. Indeed for adhesive contacts the *local* deformations result from complicate interactions occurring both over the surrounding contacting asperities as well as over the non contact areas, resulting into not easily predictable displacements.

analytical homogenization of the high-frequency content of a generic physical medium/process model is very common in physics and engineering, since it allows one to build a mean field formulation of the model itself, characterized by effective (i.e., smoother) physical properties, varying over length scales of order $\sim L_0$. This is, e.g., the case of the rough contact mechanics, where the accurate knowledge of the relationship between the effective interfacial characteristics (average interfacial separation, effective work of adhesion, etc., to cite few), plays a fundamental role in many physical processes, from friction and thermal/electrical conduction, to adhesion and interfacial fluid flow. Here we briefly describe the novel efficient numerical simulation approach devoted to simulate the contact mechanics of realistically-rough interfaces at the REV scale.

In Fig. 25 we show a schematic of the contact geometry. We assume the contact to occur under isothermal conditions, and the roughness to be characterized by a small mean square slope, in order to make use of the well-known half-space theory. Moreover, the roughness is assumed to be periodic with period L_0 in both x- and y-direction. The local separation between the mating interfaces $u(\mathbf{x})$ is shown in Fig. 25, and it can be immediately agreed to be

$$u(\mathbf{x}) = \bar{u} + w(\mathbf{x}) - h(\mathbf{x}), \tag{A1}$$

where $\bar{u}$ is the average interfacial separation, $w(\mathbf{x})$ the surface out-of-average-plane displacement and $h(\mathbf{x})$ the surface roughness, with $\langle w(\mathbf{x})\rangle = \langle h(\mathbf{x})\rangle = 0$. By defining

$$w(\mathbf{q}) = (2\pi)^{-2}\int d^2\mathbf{x}\, w(\mathbf{x})\, e^{-i\mathbf{q}\cdot\mathbf{x}}$$

and

$$\sigma(\mathbf{q}) = (2\pi)^{-2}\int d^2\mathbf{x}\, \sigma(\mathbf{x})\, e^{-i\mathbf{q}\cdot\mathbf{x}},$$

where $\sigma(\mathbf{x})$ is the distribution of interfacial pressures, it is (relatively) easy to show that $w(\mathbf{x})$ can be related to $\sigma(\mathbf{x})$ through a very simple equation in the Fourier space:

$$w(\mathbf{q}) = M_{zz}(\mathbf{q})\,\sigma(\mathbf{q}), \tag{A2}$$

where $M_{zz}(\mathbf{q}) = -2/(|\mathbf{q}|\,E_r)$ for the elastic half space [$M_{zz}(\mathbf{q})$ can be equally determined for layered or viscoelastic materials, for which the reader is referred to Ref. 50]. Finally, the relation between separation $u(\mathbf{x})$ and interaction pressure $\sigma(\mathbf{x})$ is calculated within the Derjaguin's approximation,[51] and it can be written in term of a generic interaction law $\sigma(u) = f(u)$. $f(u)$ will be repulsive for $u \le u_w$ and attractive otherwise, where u_w is a separation threshold describing the ideal equilibrium separation. In this work we have adopted the L-J potential to describe the attractive interaction, but one can equally make use of different interaction laws (e.g., the Morse potential, for chemical bonds). For $u > u_w$ (attractive side), $f(u) = f_a(u)$, where

$$f_a(u) = \frac{8}{3}\frac{\Delta\gamma}{d_c}[\varepsilon^{-9} - \varepsilon^{-3}],$$
$$\varepsilon(u) = (u - u_w + d_c)/d_c, \tag{A3}$$

otherwise (repulsive side) $f(u) = f_r(u)$ with

$$f_r(u) = \frac{8}{3}\frac{\Delta\gamma}{d_c}[\varepsilon^{-9} - \varepsilon^{-3}],$$
$$\varepsilon(u) = u/u_w. \tag{A4}$$

Usually we adopt $u_w \ll d_c$. Note however that for $u_w \to 0$ the repulsive term converges to a hard wall, whereas for $u_w = d_c$ we return to the classical (integrated) L-J interaction law.

Eqs. (A1), (A3), and (A4) are discretized on a regular square mesh of grid size δ, resulting in the following set of equations:

$$L_{ij} = -u_{ij} + (\bar{u} + w_{ij} - h_{ij}), \tag{A5}$$

$$\sigma_{ij} = f_a(u_{ij}) + f_r(u_{ij}), \tag{A6}$$

$$\sigma(x_{ij}) \to \Delta\sigma(q_{hk}) = M_{zz}^{-1}(q_{hk})w(q_{hk}) \to w(x_{ij}), \tag{A7}$$

where L_{ij} is the generic residual (related to the generic iterative solution u_{ij}). In order to solve Eqs. (A5)–(A7), we rephrase Eq. (A5) in terms of the following ideal molecular dynamics process

$$\ddot{u}_{ij} + 2\xi_{ij}\omega_{ij}\dot{u}_{ij} = \omega_{ij}^2 L_{ij}, \tag{A8}$$

which we solve with a velocity Verlet integration scheme. ξ_{ij} and ω_{ij} are, respectively, the generic damping factor and modal frequency of the residuals molecular dynamics system (RMD), which can be used to damp the error dynamics. Therefore, at equilibrium ($\ddot{u}_{ij} = \dot{u}_{ij} = 0$), Eq. (A8) returns the solution of Eqs. (A5)–(A7) at zero residuals. The adoption of the RMD scheme allows for the (ideal time) search of the solution to move in a (generic) non-physical error space to finally provide, at equilibrium, the targeted (zero residuals) solution. We have found that this very efficiently avoids to be trapped in slow relaxation dynamics and/or non-physical (non-convergent) solution as otherwise obtained with classical (usually very slow) relaxation approaches (e.g., under-relaxation, often adopted in the literature for smooth contact

conditions, see, e.g., Ref. 52) applied to realistically-rough interacting surfaces. The solution accuracy is set by requiring

$$\begin{aligned} \left\langle L_{ij}^2/u_{ij}^2\right\rangle^{1/2} &< \varepsilon_{\mathrm{L}}, \\ \left\langle\left[\left(u_{ij}^n - u_{ij}^{n-1}\right)/u_{ij}^{n-1}\right]^2\right\rangle^{1/2} &< \varepsilon_{\mathrm{u}}, \end{aligned} \tag{A9}$$

where both errors are typically of order 10^{-4}. The novelty introduced in the discussed numerical model is fundamentally related to the adoption of an augmented[53] Fourier formulation of the elastic integration in conjunction with a residuals relaxation process expressed in term of molecular dynamics in the space of lengths. Alternative numerical schemes (relevant to the simulation of realistically-rough three-dimensional contact mechanics) have been recently discussed in Refs. 18, 19, and 40. In particular, Ref. 19 improves and extends the Greenwood's relaxation scheme,[39] based on a real space formulation, by implementing the multi-integration (MI) rules for the resolution of the elastic integration problem. While MI allows a substantial lowering of the computational cost (with respect to the direct elastic integration), however, its adoption would make such a model not easily (even if possible) extendible to non-elastic (e.g., viscoelastic) interfacial responses, due to the loss of diagonal dominance of the stiffness matrix (as known, the latter is needed to enforce the MI rules). Differently from the previous scheme, in Ref. 18 the elastic response is instead calculated using a Fourier-transform technique with a linearised surface Green's function, which is embedded into an atomistic description of the contact dynamics (known as GFMD scheme). In Refs. 17 and 40, the GFMD approach is altered by adopting a continuum description for the elastic energy, whereas the relaxation (numerical damping) process is elaborated by solving the Newton's equations of motion in the Fourier space.

As anticipated in Secs. III–V, the nominal projected contact area A/A_0 is given by $A_r/A_0 + A_a/A_0$, where A_r is the area of repulsive interaction (defined by $\sigma(\mathbf{x}) > 0$), and where A_a is the area of attractive interaction (defined by $u(x) - u_w < d_c$ and $\sigma(\mathbf{x}) < 0$). In Fig. 26 we show a typical contact area map for a DMT rough interaction, where A_r/A_0 and A_a/A_0 correspond, respectively, to black and gray domains.

We also observe that for any discretized formulation of the adhesive contact mechanics, a fracture tensile stress can be related to the mesh size characteristics of the contact. To determine it, we make use of the penny-shaped crack solution (see, e.g., Ref. 6), whose tensile stress σ_a reads (the $\pi/4$ takes into account the square shape of the grid):

$$\sigma_a = \frac{\pi}{4}\sqrt{\pi\Delta\gamma E_r/\delta}.$$

Here σ_a has to be compared to the maximum tensile stress given by the interaction law, $\sigma_t = \Delta\gamma/d_c$ and, in particular, a detachment parameter $\varepsilon_a = \sigma_a/\sigma_t > 1$ in order to guarantee the convergence of the numerical solution. By adopting a Tabor number definition $\mu_{T,\lambda} = (\frac{\lambda^2}{A_\lambda(2\pi)^2}\frac{\Delta\gamma^2}{E_r^2 d_c^3})^{1/3}$, where λ is smallest roughness wavelength and A_λ the corresponding amplitude, a convergent numerical solution will be achieved if

$$n_\lambda = \lambda/\delta > \frac{32}{\pi^2}\mu_{T,\lambda}^{3/2}\left(\frac{A_\lambda}{d_c}\right)^{1/2}, \tag{A10}$$

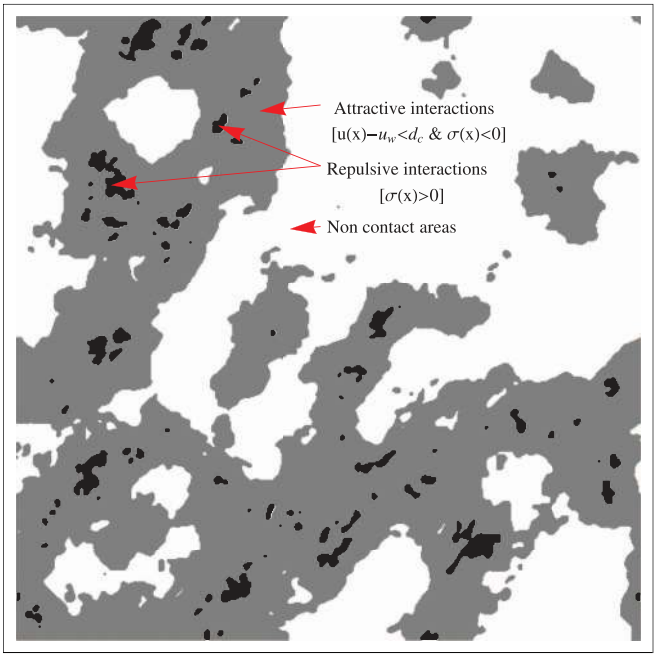

FIG. 26. Example of contact map.

where n_λ is the number of discretization points at wavelength λ. It is interesting to observe from Eq. (A10) that large Tabor numbers, i.e., adhesive interactions occurring in the full JKR regime, are numerically hard to be modelled [due to the fine mesh description required to satisfy Eq. (A10): e.g., for $\mu_{T,\lambda} = 10$ and $A_\lambda/d_c = 10^2$, we have $n_\lambda \approx 10^3$]. However, as recently shown,[40] a JKR regime can be conveniently obtained for μ_T values close to 1, reducing the computational complexity of JKR interactions.

It would be useful to test Eq. (A10) by comparing the Johnson's solution (Ref. 54, adhesive sinus contact in the JKR regime) with the corresponding numerical simulation predictions. We stress that comparing with the Westergaard geometry (in opposite to non-periodic geometry, as ball-on-flat contacts) allows to verify the numerical model in a range of contact pressures (and contact areas) which includes the Hertzian regime for small squeezing pressures, and which

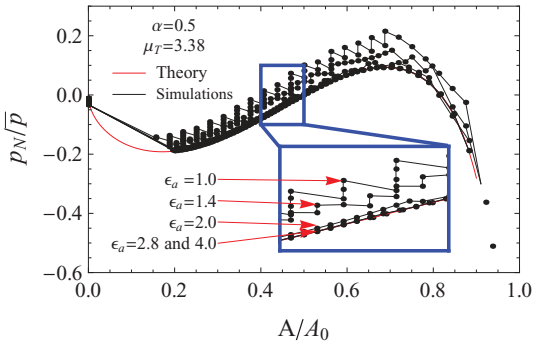

FIG. 27. Dimensionless applied pressure $p_N/\bar{p}$ as a function of the contact area, for a Westergaard like contact geometry. Red curve is from Johnson's theory, whereas dots are the corresponding numerical predictions at different detachment parameters. $\mu_{T,\lambda} = 3.4$ for all numerical results. In the magnified view, points at $\varepsilon_a = 2.8$ and 4 are superposed to the red curve.

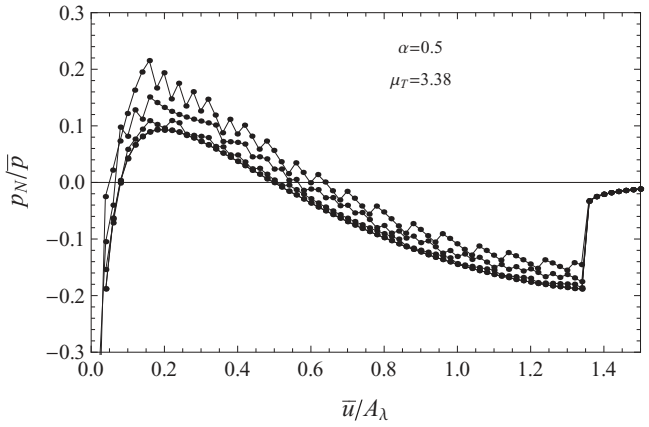

FIG. 28. Dimensionless average interfacial separation $\bar{u}/A_\lambda$ as a function of the dimensionless applied pressure $p_N/\bar{p}$, for a Westergaard like contact geometry. For the same parameters of Fig. 27.

further extends to the fracture (full contact) regime for increasing values of contact pressure. Hence, such a geometry appears the best candidate for validating the robustness of the numerical model. In particular, the relation between nominal contact pressure and contact area reads[54]

$$p_N/\bar{p} = \sin^2\phi_\alpha - \alpha\sqrt{\tan\phi_\alpha}, \qquad \text{(A11)}$$

where $\phi_\alpha = \pi A/(2A_0)$, $\alpha = \sqrt{2E_r\Delta\gamma/(\lambda\bar{p}^2)}$, and $\bar{p} = \pi E_r A_\lambda/\lambda$ (for the adhesionless interaction, $\bar{p}$ is the nominal squeezing pressure to full contact). In Fig. 27 we compare Eq. (A11) (red curve) with numerical results obtained with $\mu_{T,\lambda} \approx 3.4$ (JKR regime), at different values of detachment parameter ε_a. We stress that all the solutions shown in Fig. 27 satisfy the accuracy requirements of Eq. (A9), however only at increasing detachment parameter (in particular for $\varepsilon_a > 2$) the solution rapidly converges to the analytical one. Similar considerations apply for the pressure-separation law, shown in Fig. 28.

[1] F. P. Bowden and D. Tabor, *Friction and Lubrication of Solids* (Wiley, New York, 1956).
[2] K. L. Johnson, *Contact Mechanics* (Cambridge University Press, Cambridge, 1966).
[3] J. N. Israelachvili, *Intermolecular and Surface Forces* (Academic, London, 1995).
[4] B. N. J. Persson, *Sliding Friction: Physical Principles and Applications*, 2nd ed. (Springer, Heidelberg, 2000).
[5] B. N. J. Persson, O. Albohr, U. Tartaglino, A. I. Volokitin, and E. Tosatti, J. Phys.: Condens. Matter **17**, R1 (2005).
[6] B. N. J. Persson, Surf. Sci. Rep. **61**, 201 (2006).
[7] K. N. G. Fuller and D. Tabor, Proc. R. Soc. London, Ser. A **345**, 327 (1975).
[8] B. V. Derjaguin, V. M. Muller, and Yu. P. Toporov, J. Colloid. Interf. Sci. **53**(2), 314–326 (1975).
[9] K. L. Johnson, K. Kendall, and A. D. Roberts, Proc. R. Soc. London, Ser. A **324**, 301 (1971).
[10] J. A. Greenwood and J. B. P. Williamson, Proc. R. Soc. London, Ser. A **295**, 300 (1966).
[11] K. L. Johnson and J. A. Greenwood, J. Colloid Interface Sci. **192**, 326 (1997).
[12] D. Maugis, J. Adhes. Sci. Technol. **10**(2), 161–175 (1996).
[13] W. B. Dapp, N. Prodanov, and M. H. Müser, J. Phys.: Condens. Matter **26**, 355002 (2014).
[14] N. Prodanov, W. B. Dapp, and M. H. Müser, Tribol. Lett. **53**, 433 (2014).
[15] G. Carbone and F. Bottiglione, J. Mech. Phys. Solids **56**, 2555 (2008).
[16] C. Campana, M. H. Müser, and M. O. Robbins, J. Phys.: Condens. Matter **20**, 354013 (2008).
[17] W. B. Dapp, A. Lücke, B. N. J. Persson, and M. H. Müser, Phys. Rev. Lett. **108**, 244301 (2012).
[18] L. Pastewka and M. O. Robbins, Proc. Natl. Acad. Sci. U.S.A. **111**, 3298 (2014).
[19] S. Medina and D. Dini, Int. J. Solids Struct. **51**, 2620 (2014).
[20] N. Mulakaluri and B. N. J. Persson, EPL **96**, 66003 (2011).
[21] G. Carbone, M. Scaraggi, and U. Tartaglino, Eur. Phys. J. E **30**, 65 (2009).
[22] A. G. Peressadko, N. Hosoda, and B. N. J. Persson, Phys. Rev. Lett. **95**, 124301 (2005).
[23] B. Lorenz, B. A. Krick, N. Mulakaluri, M. Smolyakova, S. Dieluweit, W. G. Sawyer, and B. N. J. Persson, J. Phys.: Condens. Matter **25**, 225004 (2013).
[24] B. A. Krick, J. R. Vail, B. N. J. Persson, and W. G. Sawyer, Tribol. Lett. **45**, 185 (2012).
[25] K. Autumn, MRS Bull. **32**, 473 (2007).
[26] L. Heepe and S. Gorb, Annu. Rev. Mater. Res. **44**, 173–203 (2014).
[27] B. N. J. Persson, J. Chem. Phys. **118**, 7614 (2003).
[28] B. N. J. Persson and S. Gorb, J. Chem. Phys. **119**, 11437 (2003).
[29] B. N. J. Persson, C. Ganser, F. Schmied, C. Teichert, R. Schennach, E. Gilli, and U. Hirn, J. Phys. C: Condens. Matter **25**, 045002 (2013).
[30] B. N. J. Persson, A. Kovalev, and S. N. Gorb, Tribol. Lett. **50**, 17 (2013).
[31] B. N. J. Persson, J. Phys. C: Condens. Matter **19**, 376110 (2007).
[32] B. V. Derjaguin and V. Smilga, J. Appl. Phys. **38**, 4609 (1967).
[33] A. D. Roberts, J. Phys. D: Appl. Phys. **10**, 1801 (1977).
[34] B. N. J. Persson, M. Scaraggi, A. I. Volokitin, and M. K. Chaudhury, EPL **103**, 36003 (2013).
[35] K. Brörmann, K. Burger, A. Jagota, and R. Bennewitz, J. Adhes. **88**, 589–607 (2012).
[36] D. Maugis, J. Colloid Interface Sci. **150**, 243 (1992).
[37] E. Barthel, J. Phys. D: Appl. Phys. **41**, 163001 (2008).
[38] V. M. Müller, V. S. Yushenko, and B. V. Derjaguin, J. Colloid Interface Sci. **77**, 91 (1980).
[39] J. A. Greenwood, Proc. R. Soc. Lond. A **453**, 1277–1297 (1997).
[40] M. H. Müser, Beilstein J. Nanotechnol. **5**, 419 (2014).
[41] B. N. J. Persson, Eur. Phys. J. E **8**, 385 (2002).
[42] B. N. J. Persson, J. Chem. Phys. **115**, 3840 (2001).
[43] B. N. J. Persson, Phys. Rev. Lett. **99**, 125502 (2007).
[44] C. Yang and B. N. J. Persson, J. Phys. Condens. Matter **20**, 215214 (2008).
[45] A. Almqqvist, C. Campana, N. Prodanov, and B. N. J. Persson, J. Mech. Phys. Solids **59**, 2355 (2011).
[46] B. N. J. Persson, J. Phys.: Condens. Matter **20**(31), 312001 (2008).
[47] G. Carbone, B. Lorenz, B. N. J. Persson, and A. Wohlers, Eur. Phys. J. E **29**, 275 (2009).
[48] P. R. Nayak, J. Lubr. Technol. **93**, 398 (1971).
[49] In general, in order for elastic instabilities to occur in contact mechanics and sliding friction the material must be soft enough. This is most easily understood in the context of a particle in a periodic potential $U(x)$ and connected to an elastic spring k the free end of which is moving parallel to the corrugated potential (x-direction) (Tomlinson model of sliding friction). In this case energy will be dissipated in rapid slip events only if the spring is soft enough (see, e.g., Ref. 4 for a discussion of this point).
[50] B. N. J. Persson, J. Phys.: Condens. Matter **24**, 095008 (2012).
[51] B. V. Derjaguin, Kolloid Z. **69**, 155–164 (1934).
[52] C. Jin, A. Jagota, and C. Y. Hui, J. Phys. D: Appl. Phys. **44**, 405303 (2011).
[53] The term *augmented* is used to identify a novel numerical technique developed here to increase the degree of continuity (and hence of accuracy) of the solution fields. In particular, the elastic integration problem is numerically formulated in the real space in term of finite elements with linear shape function. The consequent Fourier-transform of such a finite element model allows to obtain an augmented Eq. (2), i.e., $\sigma(\mathbf{q}) = F(\mathbf{q})M_{zz}^{-1}(\mathbf{q})\,w(\mathbf{q})$, where $F(\mathbf{q})$ corresponds to the Fourier transform of the shape function. This augmented formulation can be shown to be extremely useful to damp the numerical inaccuracy resulting from the adoption of viscoelastic bulk responses. The detailed derivation of the RMD numerical model will be presented in a dedicated contribution.
[54] K. L. Johnson, Int. J. Solids Struct. **32**(3/4), 423–430 (1995).